

Effect of steel tube thickness on the behaviour of CFST columns: experimental tests and design assessment

C. Ibañez^{a*}, D. Hernández-Figueirido^b, A. Piquer^b

^aDepartment of Construction Engineering and Civil Engineering Projects, Universitat Politècnica de València, Valencia, Spain

^bDepartment of Mechanical Engineering and Construction, Universitat Jaume I, Castellón, Spain

** Corresponding autho: caribus@upv.es*

ABSTRACT

In this paper, the results of experimental tests conducted on concrete-filled steel tubular (CFST) columns are presented. There is currently a deficit of data available that can be used to evaluate current guidance documents and provide assessment to improve their accuracy when considering the behaviour of CFST columns filled with high strength concrete. Thus, this paper aims to increase the volume of experimental data available with a series of groups of tests on stub CFST columns subject to axial compression. Among the specimens of the same group only one dimension changes, the steel tube thickness. The columns are filled with both normal and high strength concrete for comparison purposes. The use of high strength concrete in circular tubes increases the concrete contribution, but this effect does not fulfil in rectangular specimens where also the confinement is less effective than in circular CFST even when the former have thin steel tubes and high strength concrete. The specifications of four commonly used codes are discussed. Comparison of their predictions with the experimental data collected shows that AISC is conservative but EC4, DBJ and AS produce similar non-conservative predictions.

Keywords: *composite stub columns; concrete-filled steel tubes; high strength concrete; sectional capacity; Eurocode 4; AISC; DBJ; AS; steel wall thickness.*

NOTATION

AISC	American Institute of Steel Construction
AS	Australian Standard
CCR	Concrete contribution ratio
CFST	Concrete-filled steel tube
DBJ	Chinese Code
DI	Ductility Index
EC4	Eurocode 4
E_s	Young's modulus of structural steel
f_c	Compressive cylinder strength (150x300 mm) of concrete (test date)
f_{cu}	Compressive cubic strength (150x150x150 mm) of concrete (test date)
f_u	Ultimate tensile strength of structural steel
f_y	Yield strength of structural steel
HSC	High strength concrete
NSC	Normal strength concrete
N_{exp}	Ultimate axial load from tests
L	Column length
SI	Strength Index
t	Thickness of the steel tube
$\bar{\lambda}$	Relative slenderness
ρ	Concrete density
ε	$\varepsilon = \sqrt{235/f_y}$

1. INTRODUCTION

Due to their very good structural performance and economic advantages, concrete-filled steel tubular (CFST) columns are widely used, among others, in high-rise buildings and large infrastructure. The composite action enhances the structural behaviour of both components which leads to members with high bearing capacities but reduced sections. The concrete core is confined by the steel tube which results in an increase in the compressive strength of the section and in its ductility. In turn, the concrete infill prevents the steel tube from local buckling, which is particularly critical in rectangular CFST columns fabricated from steel hollow sections with very thin walls.

Through various experimental programs, several authors have investigated the behaviour of CFST stub columns under axial compression (Han [1], Giakoumelis and Lam [2], Lam and Williams [3], Sakino et al. [4], Tao et al. [5], Han et al. [6], Liang and Fragomeni [7], Tahyalan et al. [8], Ekmekyapar and Al-Eliwi [9], Wang et al. [10], Patel [11]). It can be derived from these works that the composite action between the steel tube and the concrete core depends mainly on the strength of the materials, the cross-sectional size and the confining factor, notably influenced by the size-to-thickness ratio and the cross-sectional shape.

Although initially most of the works focused on normal strength concrete (NSC), the recent advances in the construction industry have made the use of high performance materials possible and, in the case of CFST columns, considerable attention has been paid to these columns filled with high-strength concrete (HSC) and numerous experimental programs have been carried out to study the behaviour of stub columns filled with HSC (Liu et al. [12], Liu [13], Liu and Gho [14], Ellobody et al. [15], Yu et al. [16], Ibañez et al. [17], Chen et al. [18]).

When subjected to heavy loads, the required column strength increases and, as a result, the cross-sectional size of the column also grows. For these members that require large dimensions, using HSC can notably reduce the column size and help to achieve a higher

resistance to weight ratio still preserving a satisfactory level of ductility and maintaining the confining action which, for higher size-to-thickness ratios, decreases due to the size effect [10]. Therefore, to meet the resistance requirements with CFST columns with reduced section, attention must be paid to the effectiveness of the confinement and the occurrence of local buckling.

Numerous examples of structures designed and built with CFST columns can already be found (e.g. the Latitude Building in Sydney [19] or the Obayashi Technical Research Institute in Japan [20] built with both high strength concrete and steel) which demonstrate the need of having reliable design codes which also take account of high performance materials in columns with reduced section. Currently, the design guidelines considering HSC for CFST columns are still limited. Due to the lack of design experience and tests results, current design codes establish certain limits on the concrete compressive strength and steel yield strength. Employing these provisions to any other CFST column out of the applicability range gives imprecise capacity predictions.

Some investigations can be found dealing with the assessment of the existing codes for predicting the ultimate strength of CFST stub columns [21] - [24]. For example, the numerical investigation carried out by Wang et al. [21] who, with a validated FE model, generated an extensive number of results to assess Eurocode 4 (EC4) [25] predictions. The predictions proved to be unsafe for thinner steel tubes and more conservative for compact sections. The discrepancy in the results confirmed the need for a more precise evaluation of the method. The authors proposed a new model with new capacity reduction factors for the materials. Previously, Tao et al. [22] conducted a similar investigation in order to evaluate the accuracy of the Australian code (AS) [26] together with the other current design codes. They found out that EC4, AS and the Chinese code (DBJ) [27] gave comparable predictions for rectangular sections but better than the American code (AISC) [28]. For circular sections, EC4 gave the best

prediction but in general, a high deviation was observed for all the codes. Also Lai and Varma [23] presented an analysis of the previous version of the AISC (from 2010). The limits of slenderness for the classification of circular CFST members for axial compression were discussed. A database of experimental results was employed and more results were added by means of an FE model. The authors stated that design equations from AISC could be used to conservatively calculate the strengths of circular CFST members.

Also it must be highlighted the recent work developed by Thai et al. [24] where limitations of design codes on material strengths and section slenderness were analysed for numerous test results on CFST stub columns, it was found that AISC gives the most conservative predictions. Especially for rectangular stub columns with slender sections in which the local buckling effect may be significant, EC4 tends to give non-conservative predictions.

In the mentioned research carried out by Thai et al. [24], experimental results from 3100 CFST stub columns were collected in an extensive database. They noted that the number of tests on high strength CFST columns is still limited compared to those of normal strength. The 22.8% of the specimens had high strength concrete between 50 and 90 MPa and only the 12.5% had concrete compressive strengths higher than 90 MPa. A similar percentage was observed in a previous publication by one authors where 539 specimens were part of a probabilistic study, and only the 39.1% had concrete compressive strength higher than 50 MPa [29].

All considered, the necessity for experimental data is evident, particularly with high strength materials, to evaluate the current codes and provide assessment to improve their accuracy. Thus, this paper aims to increase the volume of experimental data available with the performance of a series of tests on stub CFST columns subjected to axial compression. The specimens here studied can be classified into different series. Among the specimens of the same family, only one dimension changes, the steel tube thickness, being some of the tubes steel

hollow sections with considerable low thickness. The columns are filled with both normal and high strength concrete as infill for comparison purposes. In addition, the specifications of four commonly used codes (European code Eurocode 4 (EC4) [25], the Australian code (AS) [26], the Chinese code (DBJ) [27] and the American code (AISC) [28]), and are discussed and their predictions are contrasted with the experimental results so it is possible to observe if the trends detected coincide with those from other authors.

2. EXPERIMENTAL INVESTIGATION

2.1. Column specimens and test setup

A total of 18 CFST stub columns were tested under axial compression with the aim of increasing the existing data of experimental results available and assessing the specifications in the current codes. Four different series were distinguished depending of the cross-sectional shape and dimensions of the columns. For each series, only the steel tube thickness changed between the specimen with the same outer dimensions. The compressive strength of the concrete used as infill was C30 and C90 for comparison. Three different cross-sectional shapes were considered: circular, rectangular and square as shown in Fig. 1.

In Table 1, the details of all the tested columns are summarized for each series. For convenience, the test specimens were named as follows: S-D_N (i.e. C160x6₃₀), where S stands for the cross-sectional shape of the column (C for circular steel tubes, R for rectangular and S for square); D represents the cross-sectional dimensions in mm; and N is the nominal concrete strength in MPa.

This experimental program was fully carried out at the Universitat Jaume I in Castellón (Spain). All the columns were also manufactured at the laboratories of this university. Fig. 2 and Fig. 3 show some of the hollow tubes, concrete samples, and columns prepared for the tests. For the experiments, a horizontal testing frame with capacity of 5000 kN was employed as

shown in Fig. 4 together with the setup of one of the experiments. At both ends of each specimen, steel plates with dimensions 300x300x10 mm were placed. Each of these plates is screwed at the corresponding rigid piece of the load cell (100 mm thick) that assures the non-deformability of the steel plate and the proper application of the load. During the tests, all the columns had a buckling length of 300 mm with pinned-pinned (P-P) boundary conditions.

2.2. *Material properties*

2.2.1. *Hollow steel tubes*

The hollow steel tubes from which the columns were fabricated were all cold-formed carbon steel tubes, all supplied by the same manufacturer, see Fig. 2a. On account for having enough material for the coupon tests, the total length of the tubes supplied was more than strictly needed for the CFST columns. The actual values of the yield strength (f_y) were obtained through the corresponding coupon tests (3 tests per tube) and are shown in Table 1. Although the nominal yield strength of the tubes theoretically varied between S275 and S355, it can be seen in Table 1 that yield strength of some of the tubes is higher.

2.2.2. *Concrete*

In this campaign, two grades of nominal compressive strength for concrete were employed: C30 and C90. For the sake of repeatability, only commercially available materials were used for both batches, whose mix proportions are summarized in Table 2. These correspond to reliable mix proportions used by the authors in previous works [30]. All the components were put together in the mixing tank of the planetary mixer and stirred until the concrete was fully homogenized, a particularly critical task in the HSC batches given their thick consistency. In parallel with the experiments on the stub columns, the corresponding tests were carried out on the 150x300 mm cylinders to obtain the actual compressive strength (f_c) of the concrete cores. With this aim, concrete samples were prepared, Fig. 2b, and cured in standard

conditions during 28 days until the day of the test. The recorded values for the actual compressive strength are summarized in Table 1.

For the fabrication of the CFST columns, each hollow steel tube was filled with the corresponding concrete. The filling process was done by layers and each layer was compacted with the help of a vibrator rod. After the concrete was cast inside the steel tubes, the CFST columns were covered with wet plastic clothes and let to cure

3. TEST PROCEDURE AND RESULTS

3.1. Test procedure

The columns were tested to failure under axial compression. To start with, the specimens were placed horizontally in the testing frame (Fig. 4) and correctly positioned to ensure that pure compression was applied. Prior to the start of each test, the corresponding displacement control test was performed after the correct positioning of the column in the interest of the precision of the measurements. Next, the axial load was slowly applied at a rate of 1 mm/min to be able to capture in detail local folding of the CFST columns. This loading rate has proven to work properly with both the load cell and the data acquisition system so the applied displacement can be correctly controlled and the experimental results accurately recorded ([17], [30] and [31]). A displacement control protocol was used to accurately register the post-peak behaviour of the stub columns. Once the peak load was achieved, the test was planned to continue at least until the load decreased back to 85% of its peak load to measure the necessary experimental data for the posterior analysis. Due to the general ductile response of the columns, most of the experiments were easily controlled and carried out without incident. For the subsequent inspection and analysis, once the test finished, the specimen was removed and stored.

3.2. Results

Through the displacement-control machine, the response of each column was measured and registered. Fig. 5 shows two specimens after the test. The response of each stub column can be represented in a curve that shows the variation of the load with the shortening of the column during the compression test. These curves are plotted in Fig. 6 for the four series in which the experimental program is divided,

In general, most of the columns displayed a ductile response and, for these, the failure mode was local folding (outwards) of the steel tube, Fig. 5. In rectangular and square specimens, the local buckling mainly appeared in the flat sides of the cross-section (see Fig. 5b). For Series 4 in Fig. 6d, corresponding to rectangular columns R150x100, and for some specimens filled with HSC, a less ductile behaviour was observed failing shortly after the peak load, probably due to crushing of concrete. This fact evidences the less ductile response of rectangular CFST columns during the tests, especially for those with HSC, with very short decay branches in the curves. On the contrary, circular specimens from Series 1 and 2 (Fig. 6a and b) and even those square columns filled with NSC from Series 3 (Fig. 6c), exhibited a very smooth and long decay branch after the peak load, where the capacity decreases gradually, proving a more ductile behaviour.

For all the columns, increasing the compressive strength of the concrete core improves their ultimate capacity. The values of the ultimate loads, extracted from the response curves, have been summarised in Table 1 and also displayed in Fig. 7.

Regarding the influence of the steel wall thickness, it can be seen that those with low thickness show generally a less ductile response and this effect is even more notable in columns with HSC. This can be seen, for example, in Fig. 6a for Series 1 C101.3 where the column with $t=2$ mm filled with NSC (C101.6x2_30) still maintains an acceptable level of ductility,

achieving a maximum shortening in the test of 17.24 mm, whereas the equivalent column filled with HSC (C101.6x2_90) reaches only 8.46 mm after an abrupt drop of the curve.

As expected, for specimens which have an equivalent steel area (for example S125x125x4 and R150x100x4 in Table 1), the ultimate capacity of the specimens with a larger area of concrete is higher given that the concrete core is under pure compression during the axial compression test.

3.3. Strength Index

To measure the synergy existing between the steel tube and the concrete core of the CFST column, the strength index (SI) is used and it is given by the following equation:

$$SI = \frac{N_{\text{exp}}}{A_s f_y + A_c f_c} \quad (1)$$

where N_{exp} is the experimental ultimate load, A_s is the cross-sectional area of the steel tube, f_y is the yield strength of the steel tube, A_c is the cross-sectional concrete area and f_c the concrete strength. As can be observed, SI is defined as the ratio between the theoretical cross-sectional capacity and the actual ultimate load [17]. The calculated values for all the tested columns are summarized in Table 1.

In Fig. 8 it can be observed that generally an increment in the steel tube thickness leads to an increment in the SI for both NSC and HSC specimens. Only for the circular columns from Series 1 and 2 filled with NSC the SI values are usually higher than one, which corroborates that the hoop stresses appearing in these cross-sectional shapes enhance the confinement.

The HSC specimens from Series 1 C101.6 can achieve a SI value higher than one by increasing the steel tube thickness. Given the brittle nature of HSC, more area of steel is needed to increase the hoop stresses and get an effective confinement effect.

For Series 2, the specimen with HSC and the thickest wall, C160x6_90, gets as a maximum a SI equal to one. That means that, in this case, a thicker steel tube is necessary to take advantage, at least, of the theoretical capacity of the concrete core. The specimen with the steel tube that is 3 mm thick (C160x3_90) has a SI of 0.93 which means that the experimental capacity of the column is less than the theoretical and indicates that the composite action between the steel tube and the concrete core that is not enough to take fully advantage of both.

For Series 3 and 4, the specimens with square and rectangular cross-sections respectively, the SI values are always less than one, independent of the type of concrete. For these geometries, the confinement stresses are mainly localised at the corners of the cross-sections and part of the confinement effect is also due to the bending action of the flat sides, which is much less effective. The resulting SI values are less than one because, when these steel tubes start to yield, what little confinement provided by the walls is lost. This, in turn, results in the load being transferred to the steel walls, propagating further failure of the specimen. Therefore, increasing the thickness of the wall has a marked effect on the SI value of square or rectangular cross-sections.

3.4. Concrete Contribution Ratio

For each member the contribution of the concrete infill was also analysed by means of the concrete contribution ratio (CCR) as:

$$CCR = \frac{N_{\text{exp}}}{A_{s,\text{eff}} f_y} \quad (2)$$

where N_{exp} is the experimental ultimate load, f_y is the yield strength of the steel tube, and $A_{s,\text{eff}}$ is the effective cross-sectional area of the steel tube according to the Eurocode 3 model [32], which takes into account local buckling of the steel hollow tube. This expression has been already used by the authors in previous works (e.g. [17] and [31]).

Again, for the four series of the campaign the values of CCR are plotted in Fig. 9 and also summarised in Table 1. As observed for the ultimate loads, the effect of the concrete infill is much higher when HSC is employed and, more useful in circular specimens.

Considering the variation of the steel tube wall thickness, it can be seen that the values of CCR are generally higher for tubes with low thickness. This could be due to the fact that the thinner thickness of the steel tube reduces its load bearing contribution which, in turn, results in a higher contribution of the concrete core to bear the load. However, as the wall thickness increases, the value of CCR decreases since the thicker steel wall allows the steel tube to contribute to major extent to support the load.

Another beneficial effect could come from the fact the filling could prevent the local failure that may occur in thinner steel tubes, although, in this program, despite the low thickness of the walls, all the circular tubes are classified as class 1-3 according to Eurocode 3 [29], where the local buckling occurs after the material yields.

As commented previously, when the contribution of the concrete is more effective (low thickness), the CCR values achieved by columns filled with HSC are much higher because, with respect to the hollow steel tube, the failure is delayed and advantage can be taken of the higher compressive strength of the core.

For Series 4, R150x100, an increment in the wall thickness does not produce a notable effect in the concrete contribution ratio neither for NSC nor for HSC. Therefore, the increase observed in the SI values, Fig. 8, is mainly due to the steel tube itself and not to a better performance of the concrete core. Local failure in steel tubes with thicker walls is less probable to occur and, consequently, the role of the concrete core in blocking it is less significant.

3.5. Ductility Index

The third parameter used in the analysis of the results is not uniquely based in the ultimate capacity but in the load-axial shortening curves and is the ductility index (DI). The expression proposed by Han et al. [33] is adopted as suggested in other works [1]. This index is obtained as the inverse ratio between the axial shortening of the column at peak load (N_{exp}) and the axial shortening of the column corresponding to the point when it reaches back the 85% of the peak load ($N_{exp,85\%}$) in the decay branch. This parameter is calculated by the next equation:

$$DI = \frac{\delta_{85\%}}{\delta} \quad (3)$$

where δ is the axial shortening of the stub column corresponding to the peak load and $\delta_{85\%}$ is the axial shortening of the column when the load has fallen to the 85% of the peak load.

In Table 1 the calculated values for DI are recapitulated. As can be seen the ductility index could not be calculated for some of the specimens filled with NSC. In these cases, the duration of the experiment was not compatible with the specifications of the equipment and it was necessary to stop it before the decay branch of the response curve decreased back the 85% of the peak. However, the fact that it took so long to reach $N_{exp,85\%}$ denotes the considerable ductility of these columns (C100x3_30, C100x5_30 and C160x6_30 in Fig. 6a and Fig. 6b respectively) that combine NSC with thicker steel circular tubes.

As an example, in Fig. 10a, the extraction of the values required for the calculation of DI is shown schematically for column C101.6x5_90 from Series 1. The comparison for the four series of the experimental program is shown in Fig. 10b. As expected, the DI values are higher for NSC which agrees with the different shape of the compression load-shortening curves for each type of concrete. In comparison with the flat shape detected in NSC specimens, for HSC columns the transition from the pre-peak to the post-peak is very sharp and rough, especially for Series 3 and 4 with square and rectangular columns. In these cases, a clear trend in function

of the wall thickness cannot be extracted given the irregular shape of the decay branch of the load-axial shortening curves.

4. COMPARISON OF RESULTS WITH CODE PREDICTIONS

Current design codes establish certain limits on the concrete compressive strength and section slenderness since still the number of test results on specimens combining these characteristics is insufficient to establish a reliable method. In this section, the design methods proposed by four of the most commonly used design codes are compared with the test results to check the accuracy of their prediction on stub CFST columns with HSC and different wall tube thickness.

The design approaches included in this analysis are the European code Eurocode 4 EN1994-1-1 (EC4) [25], the American code (AISC) [28], the Chinese code DBJ 13-51-2010 (DBJ) [27] and the Australian code AS5100 (AS) [26]. Firstly, a brief description of each approach is given. In parallel, a summary of the key parts of the analysed methods for the axial capacity of circular and rectangular stub columns as well as their limitations can be observed in Table 3.

For the analysis accomplished in this paper, since both, the yield strength of the steel tubes and the compressive strength of the concrete cores, are known, all the material safety factors specified in the different codes are set to one.

As can be seen in Table 3, the equations to calculate the sectional capacity (squash load) of CFST columns adopted by the design codes analysed are different, although all are based on the sum of the resistances provided by the concrete core and the steel tube. The confinement effect of the concrete core depends on the material strengths, shape and column slenderness and on the size-to-thickness ratio but is only taken into account by some codes.

The assessment of the different approaches is done taking as a reference the experimental capacities and the results are presented in Table 4 and shown graphically in Fig. 11. The expression presented next is used to obtain the prediction error:

$$\xi = \frac{N_{\text{exp}}}{N_{\text{code}}} \quad (4)$$

where N_{exp} is the experimental ultimate capacity and N_{code} is the sectional capacity predicted by the corresponding code.

With the errors obtained, the influence of the section slenderness on the predictions is analysed in Fig. 12 and Fig. 13 for circular and rectangular columns respectively.

4.1.1. Eurocode 4

The Eurocode 4 (EC4) [25] deals with the design of composite members and presents a different model in function of the cross-sectional shape. The capacity of the stub column is obtained directly as the sum of the contribution of each material for rectangular sections but for circular sections, the concrete contribution is enhanced and the steel capacity reduced in the case of concentric axial load and relative slenderness under 0.50.

The results obtained by this method are shown in Table 4 (N_{EC4}) together with the error calculated with respect to the experimental values. In Fig. 11a, the values are plotted against the wall thickness. EC4 gives generally non-conservative predictions with a mean of 0.87, being particularly on the unsafe side for specimens with square or rectangular cross-sections. This observation coincides with that detected first by Wang et al. [21] and later by Thai et al. [24] in their recent work based in the analysis of 1318 tests on short columns involving circular and rectangular sections. The calculated capacities tend to be safer with an increase in the steel wall thickness, when the section slenderness increases. This can also be seen in Fig. 12a and Fig. 13a for circular and rectangular columns respectively. Although, in this case, all the specimens

are inside the limitation of section slenderness, the closer to the limit, the less conservative the predictions.

4.1.2. *American Institute of Steel Construction*

The expressions proposed by the AISC [28] for the design of composite columns depends on the shape and the ratio of maximum dimension to thickness. The code considers high strength concrete (up to 70 MPa) and permits to increase the concrete core strength only for circular sections due to confinement, see Table 3. In addition, the effect of cross-sectional slenderness is included in the expression for the nominal axial capacity of stub columns.

In Table 4, the predictions obtained (N_{AISC}) as well as the error are shown. From Fig. 11b it can be seen that for all the columns, the predictions are safer for columns fabricated from thicker steel tubes, and that AISC produces safer results than EC4 with a mean of 1.03, being more conservative for circular sections. This trend is also corroborated by that presented in the work developed by Thai et al. [24].

In Fig. 12b and Fig. 13b it is observed that all the cases analysed are characterised as compact sections according to the code. The predictions for those specimens that are closer to being defined as non-compact sections are less conservative and, in the case of square and rectangular sections, the error values lie even beyond the 15% boundary.

4.1.3. *Chinese standard*

The experimental ultimate loads were compared to the maximum load calculated according to the design method proposed by Chinese standard code [27] for composite members. As can be seen in Table 3, DBJ bases its method on the definition of an equivalent material for the composite section. The influence of high strength concrete and the size-to-thickness ratio are considered.

The calculated values (N_{DBJ}) given by DBJ are presented in Table 4 and Fig. 11c and are considerably unsafe, being beyond the 15% error boundary for most of the cases, including some circular columns. Thus, the mean value is unsafe and has the lowest value of all the four codes studied. As observed by other authors [22], the DBJ predictions are similar to those given by EC4 and AS.

Despite the unsafe predictions, DBJ places the specimens far from the cross-sectional slenderness limit both for circular (Fig. 12c) and for rectangular (Fig. 13c). Only for the specimens C101.6x5 from Series 1, with the lowest section slenderness, does the code give conservative predictions.

4.1.4. Australian Standard

The model presented in the Australian Standard [26] is analogous to the EC4 approach. The resistance of square and rectangular CFST columns is obtained by the sum of the individual capacities of the components and, for circular columns specifically, the confinement action is considered. Consequently, the predicted capacities are very similar to those given by the European code. A non-conservative trend is observed (mean error 0.88), with more conservative values for thicker tubes.

In Fig. 12d and Fig. 13d, the influence of the cross-sectional slenderness on the results is studied. In the case of AS and circular sections (Fig. 12d) it can be observed how the predictions are unsafe for those columns placed by the code beyond the section slenderness limit. For square and rectangular sections, the calculated values are non-conservative in all cases, but specially for the specimens R150x100x4_90 from Series 4 which lie out of the 15% border.

5. SUMMARY AND CONCLUSIONS

In this paper, a series of tests on 18 concrete-filled steel tubular (CFST) stub columns subjected to concentric loads are described. Each series was characterized by the shape and size

and, for each one, two types of concrete strength were combined with different thicknesses of the steel tube. The influence of concrete infill and steel tube thickness as well as the composite action and the level of ductility were studied. Finally, the current code provisions were compared with the experimental ultimate loads. From this work, several aspects are worth noting:

- The mode of failure was local buckling of the steel tube. The behaviour of columns with high strength concrete (HSC) and thinner tubes was less ductile, particularly for square and rectangular cross-sections. In circular CFST columns, even those with thin steel tubes, strength index (SI) values of greater than one can be achieved due to the confinement effect of the steel tube. For rectangular sections, the confinement provided by the steel tubes is however far less pronounced. This conclusion corroborates the results given by other authors.
- These new experimental results confirm that, as expected, using HSC as infill in circular steel tubes greatly increased the concrete contribution ratio (CCR), even with thinner steel tubes. However, for rectangular specimens, an increase in the steel tube thickness did not result in an increase in the concrete contribution.
- The predictions given by EC4, AISC, DBJ and AS standards were assessed. Comparisons showed that AISC gives the most conservative results, especially for thicker circular steel tubes. EC4, DBJ and AS produce similar non-conservative predictions. Even though the sections studied, despite having small wall thicknesses, are not classified as slender, non-conservative predictions are obtained, especially closer to the section slenderness limitation $D/(t \cdot \epsilon)$.
- Although the number of tests in this program is limited, the results obtained serve to increase the volume of data available for comparison and validation, and corroborate the trends observed by other authors in more extensive studies (Wang

et al. [21], Tao et al. [22], Thai et al. [24]). The results support the conclusion that more tests to evaluate the accuracy of the current guidance in predicting the capacity of stub CFST columns, and to assess the applicability of the current section slenderness limitations are required.

ACKNOWLEDGEMENTS

The authors would like to express their sincere gratitude to Universitat Jaume I for the funding provided through the projects P1-1A2015-06 and UJI-B2018-58.

REFERENCES

- [1] Han LH. Tests on stub columns of concrete-filled RHS sections. *Journal of Constructional Steel Research* 2002; 58 (3):353–372.
- [2] Giakoumelis G, Lam D. Axial capacity of circular concrete-filled tube columns. *Journal of Constructional Steel Research* 2004; 60: 1049–1068.
- [3] Lam D, Williams CA. Experimental study on concrete filled square hollow sections. *Steel and Composite Structures* 2004; 4 (2):95–112.
- [4] Sakino K, Nakahara H, Morino S, Nishiyama I. Behavior of centrally loaded concrete-filled steel-tube short columns. *Journal of Structural Engineering* 2004; 130(2): 180–188.
- [5] Tao Z, Han LH, Wang ZB. Experimental behaviour of stiffened concrete-filled thin-walled hollow steel structural (HSS) stub columns. *Journal of Constructional Steel Research* 2005; 61: 962–983.
- [6] Han LH, Yao GH, Zhao XL. Tests and calculations for hollow structural steel (HSS) stub columns filled with self-consolidating concrete (SCC). *Journal of Constructional Steel Research* 2005; 61(9): 1241–1269.
- [7] Liang QQ, Fragomeni S. Nonlinear analysis of circular concrete-filled steel tubular short columns under axial loading. *Journal of Constructional Steel Research* 2009; 65(12): 2186–2196.
- [8] Thayalan P, Aly T, Patnaikuni I. Behaviour of concrete-filled steel tubes under static and variable repeated loading. *Journal of Constructional Steel Research* 2009; 65(4):900–908.

- [9] Ekmekyapar T, Al-Eliwi B. Experimental behaviour of circular concrete filled steel tube columns and design specifications. *Thin-Walled Structures* 2016; 105: 220–230.
- [10] Wang W, Ma H, Li Z, Tang Z. Size effect in circular concrete-filled steel tubes with different diameter-to-thickness ratios under axial compression. *Engineering Structures* 2017; 151: 554–567.
- [11] Patel VI. Analysis of uniaxially loaded short round-ended concrete-filled steel tubular beam-columns. *Engineering Structures* 2020; 205:110098.
- [12] Liu D, Gho WM, Yuan J. Ultimate capacity of high-strength rectangular concrete-filled steel hollow section stub columns. *Journal of Constructional Steel Research* 2003; 59: 1499–1515.
- [13] Liu D. Tests on high-strength rectangular concrete-filled steel hollow section stub columns. *Journal of Constructional Steel Research* 2005; 61: 902–911.
- [14] Liu D, Gho WM. Axial load behaviour of high-strength rectangular concrete-filled steel tubular stub columns. *Thin-Walled Structures* 2005; 43: 1131–1142.
- [15] Ellobody E, Young B, Lam D. Behaviour of normal and high strength concrete-filled compact steel tube circular stub columns. *Journal of Constructional Steel Research* 2006; 62(7): 706–715.
- [16] Yu Q, Tao Z, Wu YX. Experimental behaviour of high performance concrete-filled steel tubular columns. *Thin-Walled Structures* 2008; 46: 362–370.
- [17] Ibañez C, Hernández-Figueirido D, Piquer A. Shape effect on axially loaded high strength CFST stub columns. *Journal of Constructional Steel Research* 2018; 147: 247–256.
- [18] Chen S, Zhang R, Jia LJ, Wang JY, Gu P. Structural behavior of UHPC filled steel tube columns under axial loading. *Thin-Walled Structures* 2018; 130: 550–563.
- [19] Chaseling C. Star attraction. *Modern Steel Construction* 2004; 44 (12): 36–42.

- [20] Liew JYR, Xiong MX, Xiong DX. Design of high strength concrete filled tubular columns for tall buildings. *International Journal of High-Rise Buildings* 2014; 3 (3): 215–221.
- [21] Wang ZB, Tao Z, Han LH, Uy B, Lam D, Kang WH. Strength, stiffness and ductility of concrete-filled steel columns under axial compression. *Engineering Structures* 2017; 135: 209–221.
- [22] Tao Z, Uy B, Han LH, He SH. Design of concrete-filled steel tubular members according to the Australian Standard AS 5100 model and calibration. *Australian Journal of Structural Engineering* 2008; 8(3):197–214.
- [23] Lai ZC, Varma AH. Noncompact and slender circular CFT members: Experimental database, analysis, and design. *Journal of Constructional Steel Research* 2015; 106: 220–233.
- [24] Thai S, Thai HT, Uy B, Ngo T. Concrete-filled steel tubular columns: Test database, design and calibration. *Journal of Constructional Steel Research* 2019; 157: 161–181.
- [25] CEN EN 1994-1-1. Eurocode 4: Design of composite steel and concrete structures. Part 1-1: General rules and rules for buildings. Brussels, Belgium: Comité Européen de Normalisation; 2004.
- [26] AS/NZS2327: Composite Structures-Composite steel-concrete construction in Buildings. Australian Standard; 2017.
- [27] DBJ13-51-2010: Technical specification for concrete-filled steel tubular structures. Fuzhou, China. The Construction Department of Fujian Province; 2010.
- [28] AISC-360-16: Specification for Structural Steel Buildings. Chicago, USA. American Institute of Steel Construction; 2016.

- [29] Pavia E, Hernandez-Figueirido D, Gardoni P. Probabilistic sectional capacity models for rectangular concrete-filled steel, columns based on experimental observations. 8th International Conference on Steel and Aluminium Structures, Hong Kong, 2016.
- [30] Piquer A, Ibañez C, Hernández-Figueirido D. Structural response of concrete-filled round-ended stub columns subjected to eccentric loads. *Engineering Structures* 2019; 184: 318–328.
- [31] Hernández-Figueirido D, Romero ML, Bonet JL, Montalvá JM. Ultimate capacity of rectangular concrete-filled steel tubular columns under unequal load eccentricities. *Journal of Constructional Steel Research* 2012; 68(1): 107–117.
- [32] CEN EN 1993-1-1. Eurocode 3: Design of steel structures. Part 1.1: General rules and rules for buildings. Brussels, Belgium: Comité Européen de Normalisation; 2005.
- [33] Han LH, Zhao XL, Tao Z. Tests and mechanics model for concrete filled SHS stub columns, columns and beam-columns. *Steel & Composite Structures – An International Journal* 2001; 1(1): 51–74.

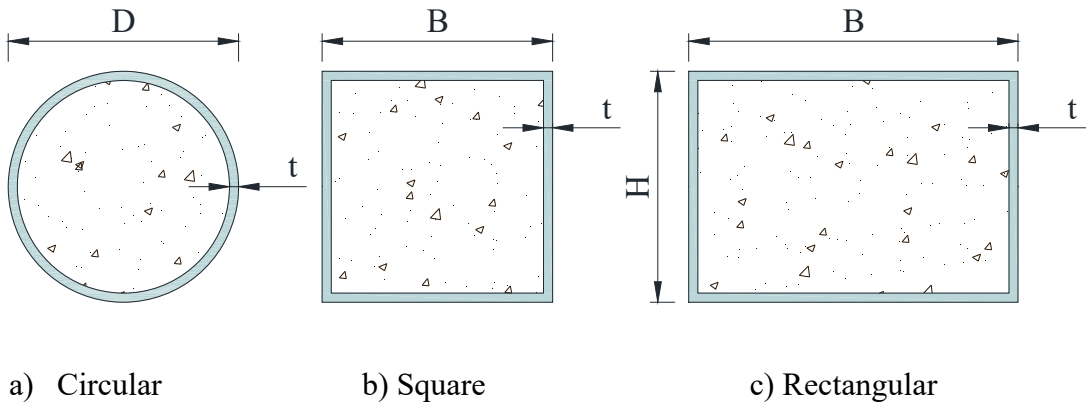


Fig. 1. Concrete filled steel tubular sections studied: a) Circular; b) Square; c) Rectangular.

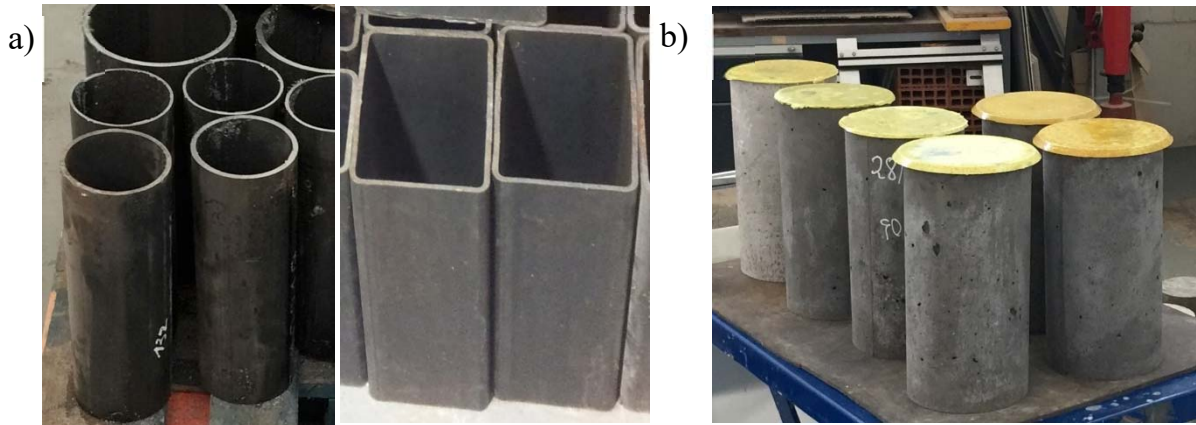


Fig. 2. a) Hollow steel tubes; b) Concrete cylinder samples.



Fig. 3. Specimens ready to be tested.

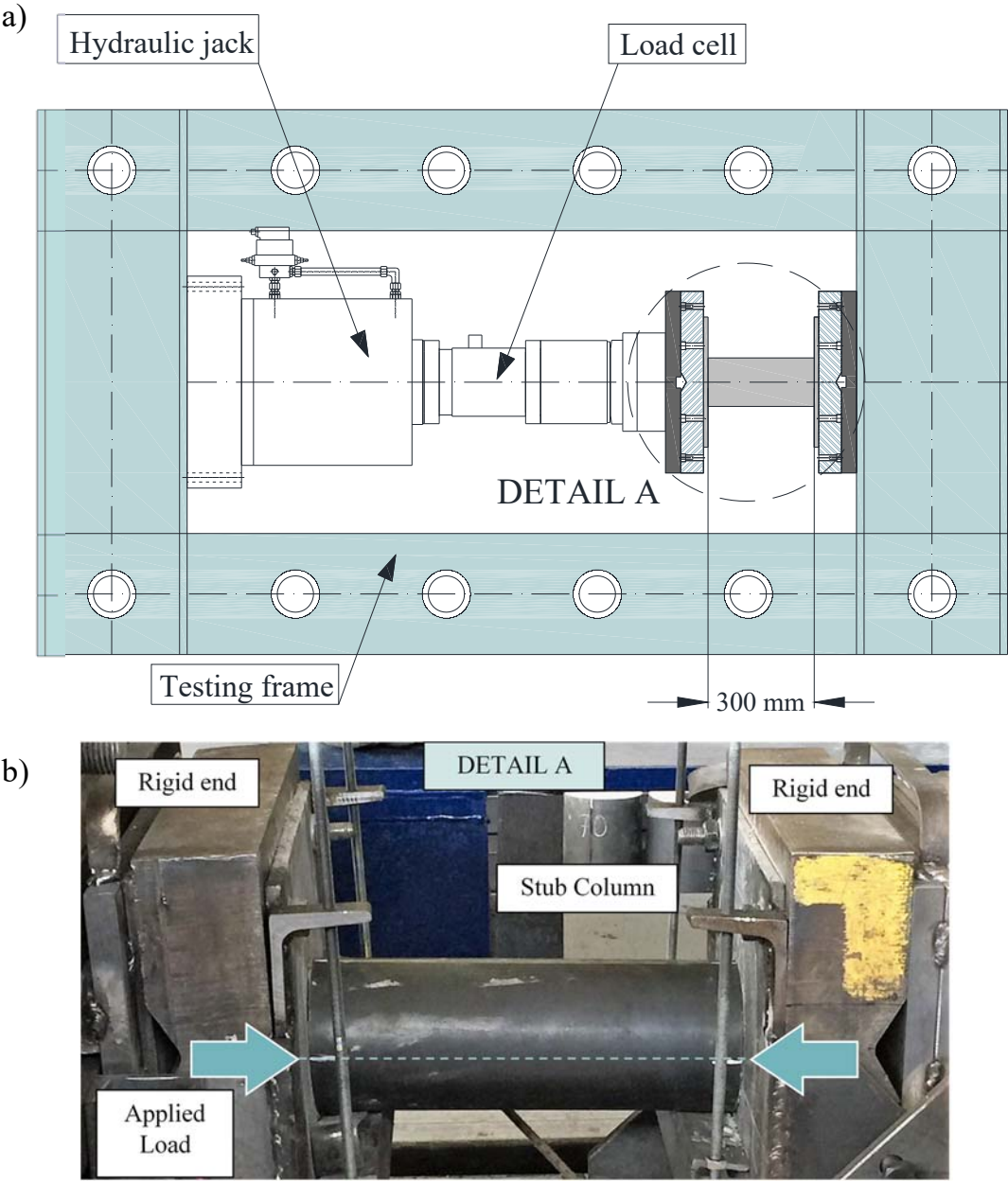


Fig. 4. a) Scheme of test setup; b) Detail of the test setup for one of the columns (Detail A).

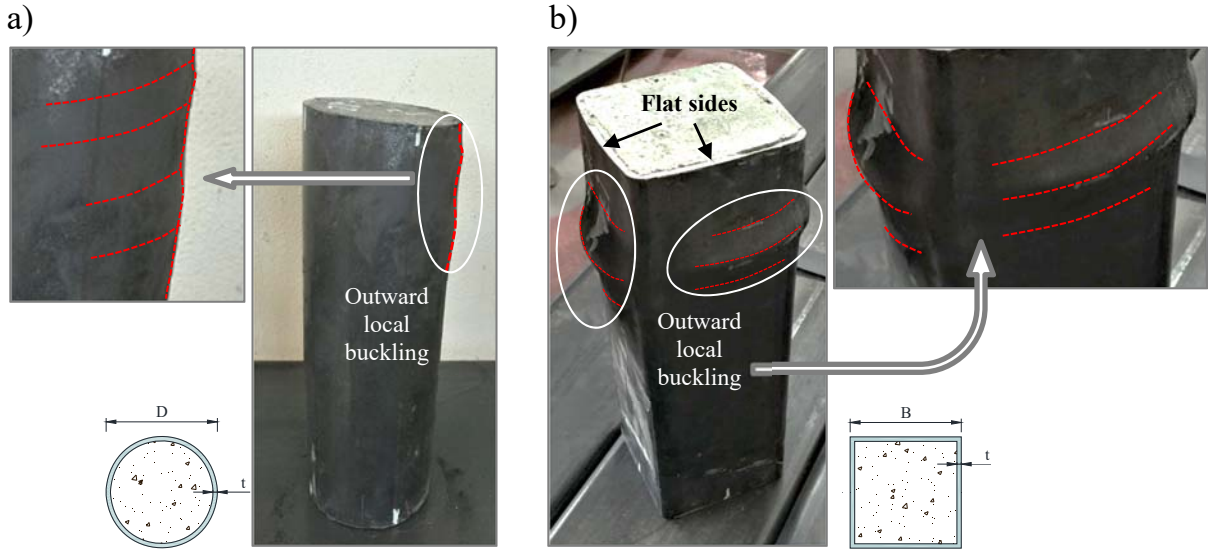


Fig. 5. Typical failure mode: a) C101.6x5_90; b) S125x125x4_30.

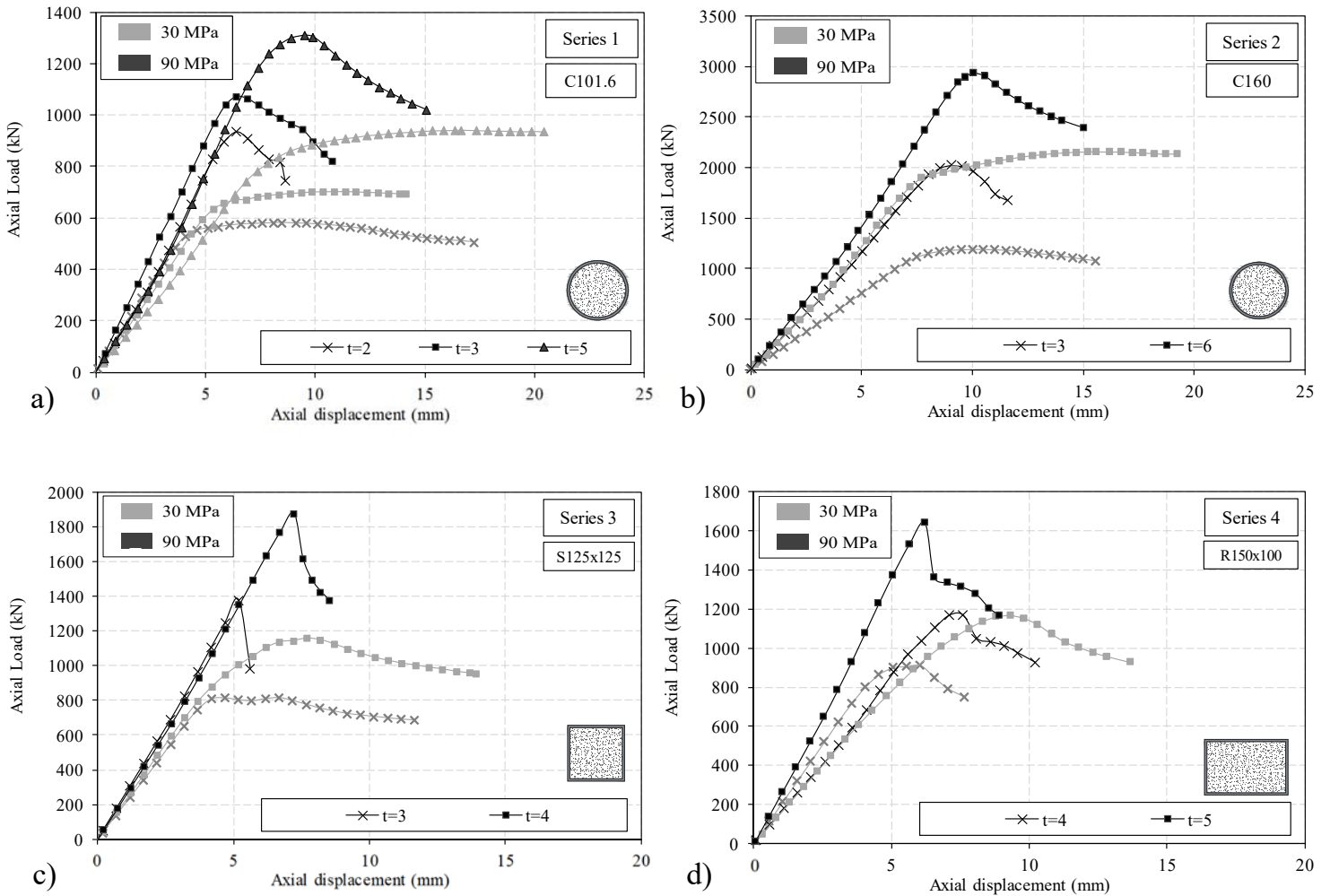


Fig. 6. Compression load versus shortening for: a) series 1, b) series 2, c) series 3, d) series 4.

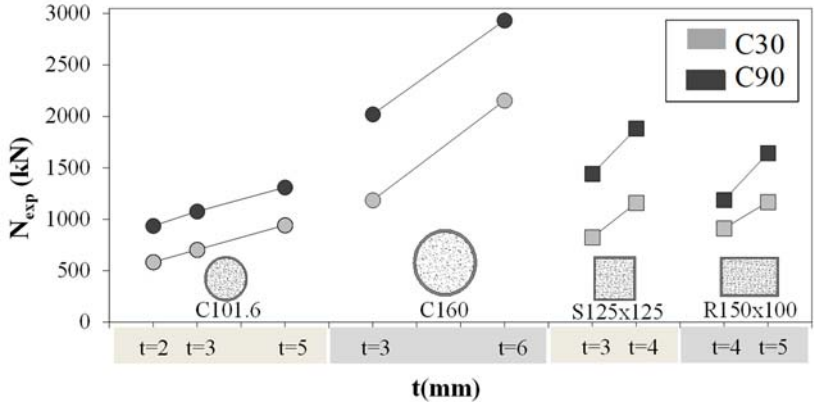


Fig. 7. Maximum load (N_{exp}).

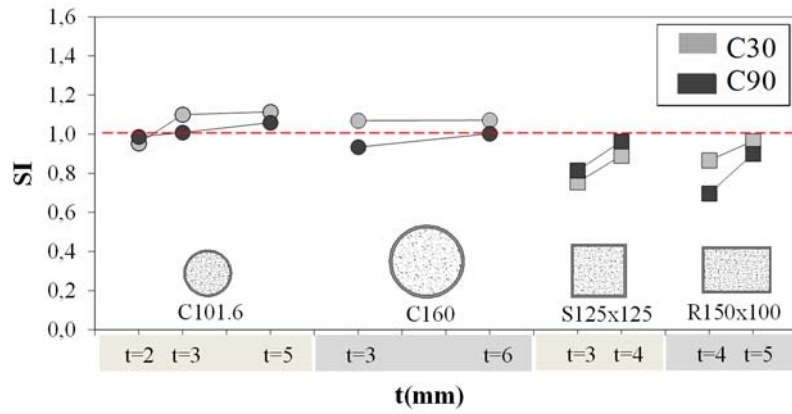


Fig. 8. Strength Index (SI).

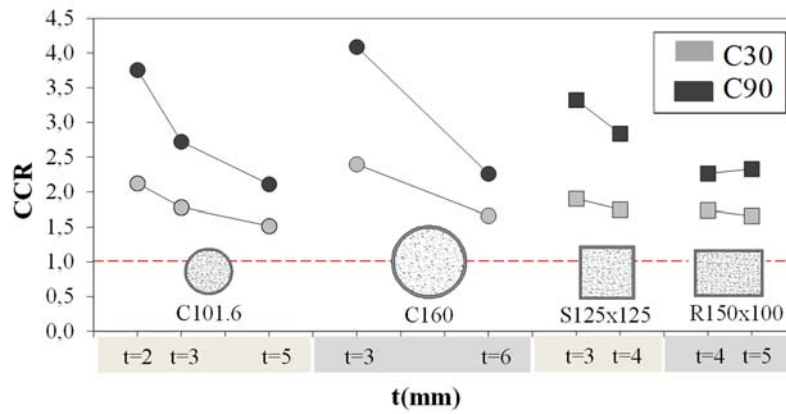


Fig. 9. Concrete contribution ratio (CCR).

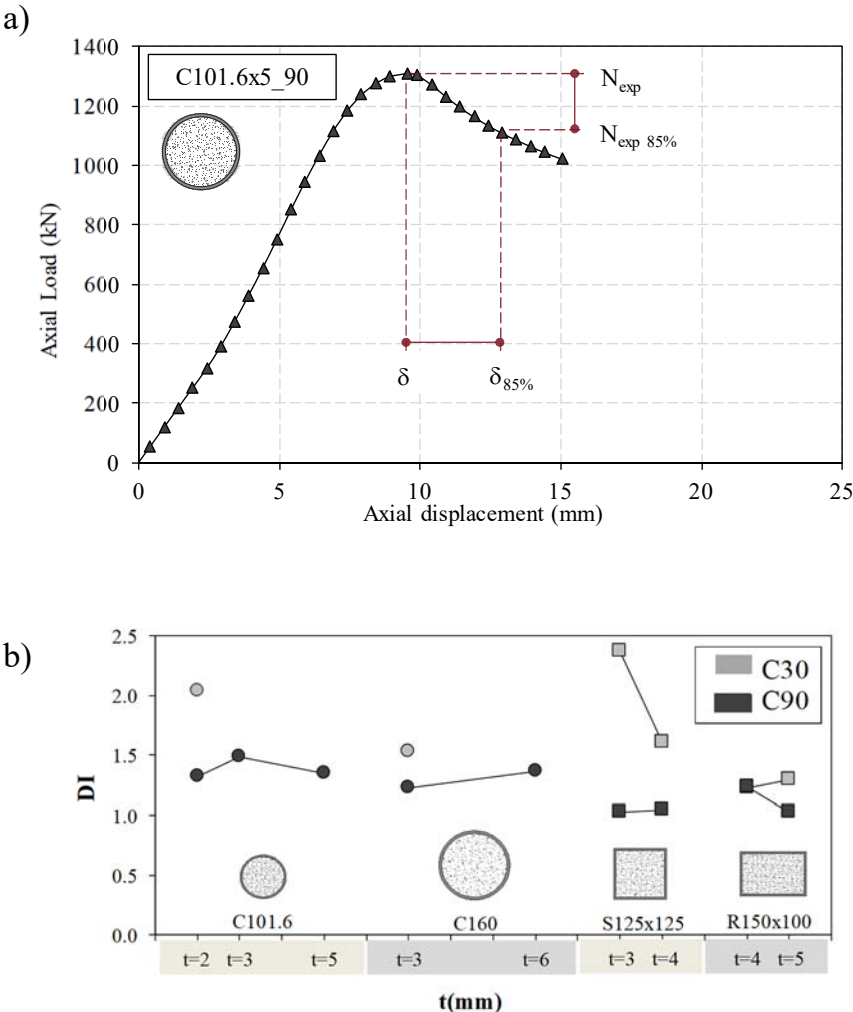


Fig. 10. a) Determination of ductility index from load-shortening curves; b) Ductility Index (DI).

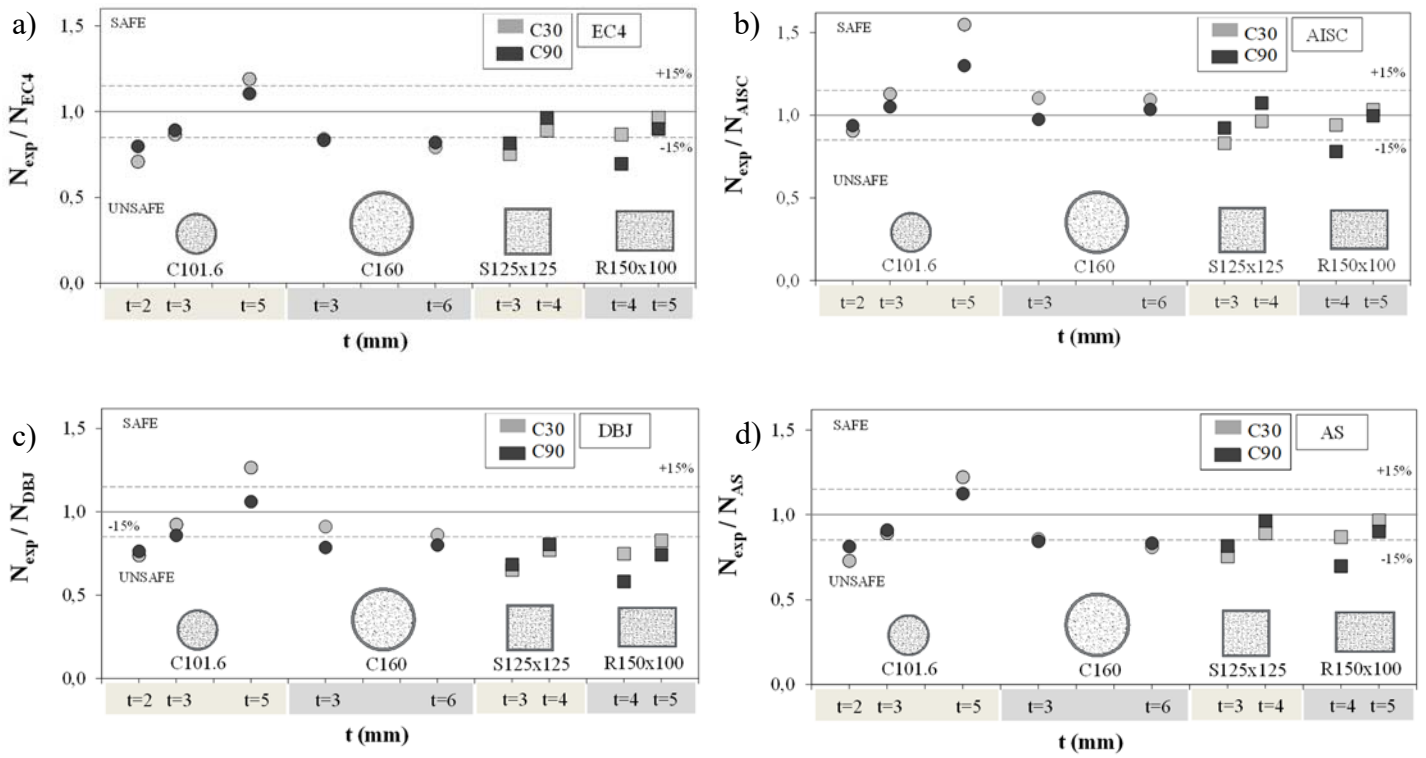


Fig. 11. Comparison between the predicted and measured cross-sectional strength.

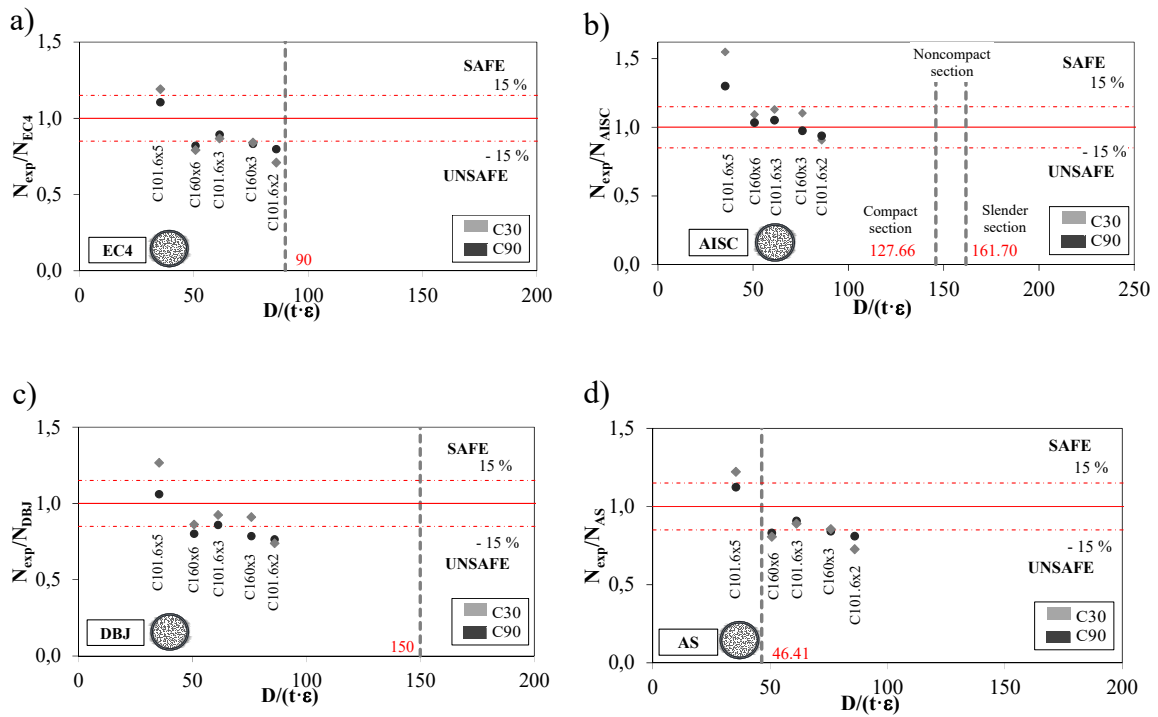


Fig. 12. Circular columns. Influence of section slenderness on code predictions.

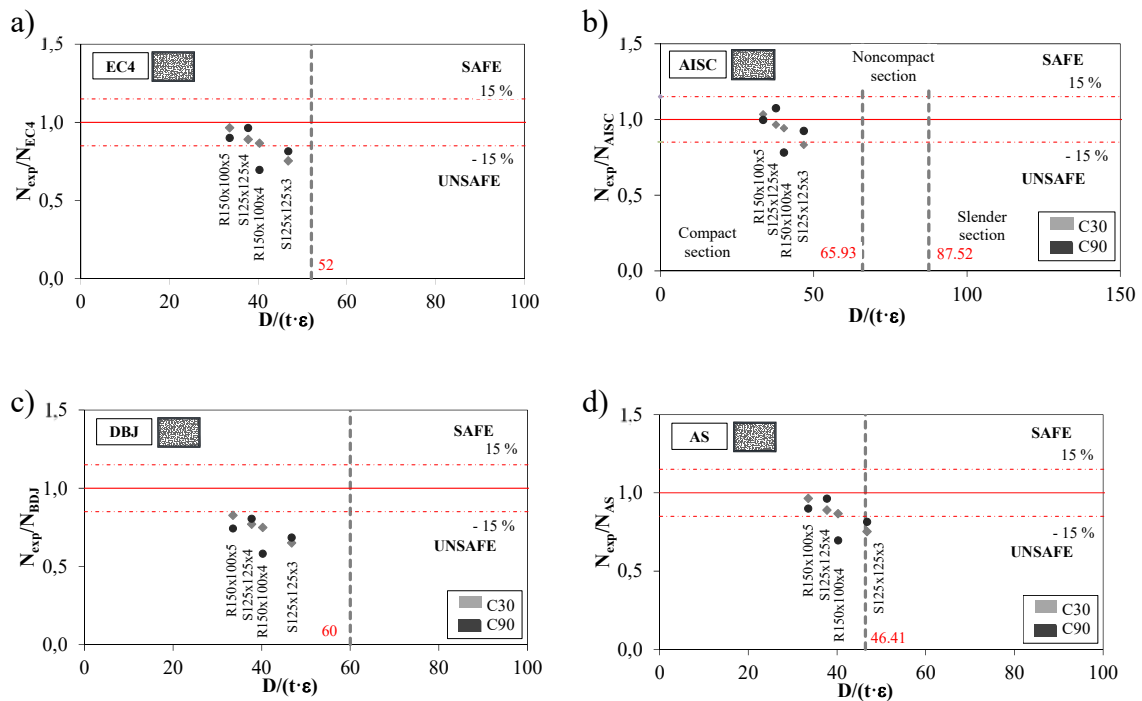


Fig. 13. Rectangular columns. Influence of section slenderness on code predictions.

Table 1. Details of the column specimens and test results

Series	Name	Dim. (mm)	t (mm)	A _s (mm ²)	A _c (mm ²)	f _y (MPa)	f _u (MPa)	E _s (GPa)	f _c (MPa)	N _{exp} (kN)	δ (mm)	δ _{85%} (mm)	SI	CCR	DI
1	C101.6x2_30	101.60	2	625.8	7482	397.94	410.91	297	40.8	582.7	8.47	17.24	0.95	2.12	2.04
	C101.6x3_30	101.60	3	929.3	7178	425.03	465.95	133	34.04	703.3	11.26	-	1.10	1.78	-
	C101.6x5_30	101.60	5	1517	6590	409.35	439.35	134	34.04	942.2	16.63	-	1.11	1.52	-
	C101.6x2_90	101.60	2	625.8	7482	397.94	410.91	297	93.51	935.7	6.41	8.46	0.99	3.76	1.32
	C101.6x3_90	101.60	3	929.3	7178	425.03	465.95	133	93.51	1075.5	6.58	9.79	1.01	2.72	1.49
	C101.6x5_90	101.60	5	1517	6590	409.35	439.35	134	93.51	1311.0	9.54	12.83	1.06	2.11	1.34
2	C160x3_30	159.00	3	1470	18385	336.28	353.09	149	33.39	1185.7	10.19	15.57	1.07	2.40	1.53
	C160x6_30	160.00	6	2903	17203	446.91	456.655	131	41.44	2154.5	15.56	-	1.07	1.66	-
	C160x3_90	159.00	3	1470	18385	336.28	353.09	149	90.85	2021.7	9.09	11.14	0.93	4.09	1.23
	C160x6_90	160.00	6	2903	17203	446.91	456.655	131	94.68	2933.2	10.05	13.67	1.00	2.26	1.36
3	S125x125x3_30	125x125	3	1464	14161	296.06	312.16	197	46.67	824.5	4.49	10.63	0.75	1.90	2.37
	S125x125x4_30	125x125	4	1936	13689	342.59	360.95	160	46.67	1159.2	7.70	12.37	0.89	1.75	1.61
	S125x125x3_90	125x125	3	1464	14161	296.06	312.16	197	94.33	1441.2	5.54	5.67	0.81	3.33	1.02
	S125x125x4_90	125x125	4	1936	13689	342.59	360.95	160	94.33	1882.5	7.27	7.58	0.96	2.84	1.04
4	R150x100x4_30	150x100	4	1936	13064	270.84	283.50	240	40.41	912.0	5.91	7.22	0.87	1.74	1.22
	R150x100x5_30	150x100	5	2400	12600	293.56	310.82	248	40.19	1168.0	9.31	12.02	0.96	1.66	1.29
	R150x100x4_90	150x100	4	1936	13064	270.84	283.50	240	90.58	1188.5	7.38	9.12	0.70	2.27	1.24
	R150x100x5_90	150x100	5	2400	12600	293.56	310.82	248	88.92	1641.8	6.20	6.34	0.90	2.33	1.02

Table 2. Concrete mix proportions

Type of infill	C30	C90
Cement (kg/m ³)	348	570
Water (l/m ³)	220	180
Sand (kg/m ³)	1065	705
Gravel (kg/m ³)	666	890
Silica fume (kg/m ³)	-	50
Superplasticizer (kg/m ³)	-	12.3

Table 3. Code prediction methods and limitations

	Materials		Local buckling		Prediction of ultimate capacity	
	Steel f_y (MPa)	Concrete f_c (MPa)	Circular	Rectangular	Circular	Rectangular
EC4 [25]	$235 \leq f_y \leq 460$ $E_a = 210\text{GPa}$	$25 \leq f_c \leq 50$ $E_c = 22000 \left(\frac{f_c}{10}\right)^{0.3}$	$\frac{D}{t} \leq 90\epsilon^2$	$\frac{H}{t} \leq 52\epsilon$	$N_{EC4} = \eta_a A_s f_y + \left(1 + \eta_c \frac{t}{D} \frac{f_y}{f_c}\right) A_c f_c$ $\eta_a = 0.25(3 + 2\bar{\lambda}) \leq 1$ $\eta_c = 4.9 - 18.5\bar{\lambda} + 17\bar{\lambda}^2 \geq 0$	$N_{EC4} = A_s f_y + A_c f_c$
					$N_{AISC} = N_0 0.658^{\frac{N_0}{N_{cr}}}$	
					$N_0 = P_p = A_a \cdot f_y + \alpha \cdot A_c \cdot f_c$ if $\lambda \leq \lambda_p$	
					$N_0 = P_p - \frac{P_p - P_y}{(\lambda_r - \lambda_p)^2} \cdot (\lambda - \lambda_p)^2$ if $\lambda_p < \lambda \leq \lambda_r$	
					$N_0 = A_a \cdot F_{cr} + 0.70 \cdot A_c \cdot f_c$ if $\lambda > \lambda_r$	
AISC [28]	$f_y \leq 525$ $E_a = 200\text{GPa}$	$21 \leq f_c \leq 70$ $E_c = 0.043\rho^{1.5} \sqrt{f_c}$	$\lambda_p = 0.15 \frac{E_a}{f_y}$ $\lambda_p = 127.66\epsilon^2$	$\lambda_p = 2.26 \sqrt{\frac{E_a}{f_y}}$ $\lambda_p = 65.93\epsilon$	$F_{cr,CCFT} = \left(\frac{0.72 \cdot f_y}{\left(\frac{D}{t} \cdot \frac{f_y}{E_s}\right)^{0.20}} \right)$ $\alpha_{circular} = 0.95$	$F_{cr,RCFT} = \frac{9 \cdot E_a}{\lambda^2}$ $\alpha_{circular} = 0.95$
					$P_y = A_a \cdot f_y + 0.7 \cdot A_c \cdot f_c$	
					$\lambda_{CCFT} = \frac{D}{t}$ $\lambda_{RCFT} = \frac{B}{t}$	
					$\lambda_{p,CCFT} = 0.15 \cdot \frac{E_a}{f_y}$ $\lambda_{r,CCFT} = 0.19 \cdot \frac{E_a}{f_y}$ $\lambda_{max,CCFT} = 0.31 \cdot \frac{E_a}{f_y}$	
					$\lambda_{p,RCFT} = 2.26 \cdot \sqrt{\frac{E_a}{f_y}}$ $\lambda_{r,RCFT} = 3.00 \cdot \sqrt{\frac{E_a}{f_y}}$ $\lambda_{max,RCFT} = 5.00 \cdot \sqrt{\frac{E_a}{f_y}}$	
DBJ [27]	$235 \leq f_y \leq 420$ $E_a = 206\text{GPa}$	$30 \leq f_{cu}^{150} \leq 90$ $E_c = \frac{10^5}{2.2 + \frac{34.7}{\rho}}$	$\frac{D}{t} \leq 150 \frac{235}{f_y}$ $\frac{D}{t} \leq 150\epsilon^2$	$\frac{H}{t} \leq 60 \sqrt{\frac{235}{f_y}}$ $\frac{H}{t} \leq 60\epsilon$	$N_{DBJ} = f_{sc}(A_s + A_c)$ $\xi_0 = \frac{A_s \cdot f_y}{A_c \cdot f_c}$	$f_{sc,circular} = (1.14 + 1.02\xi_0) f_c$ $f_{sc,rect} = (1.18 + 0.85\xi_0) f_c$
AS [26]	$f_y \leq 450$ $E_a = 200\text{GPa}$	$25 \leq f_c \leq 65$ $E_c = 0.043\rho^{1.5} \sqrt{f_c}$	$\frac{D}{t} \sqrt{\frac{f_y}{250}} \leq 82$ $\frac{D}{t} \leq 87.23\epsilon^2$	$\frac{H}{t} \cdot \sqrt{\frac{f_y}{250}} \leq$ $\begin{cases} 45 & \text{hot} \\ 40 & \text{cold} \\ 35 & \text{welded} \end{cases}$	$N_{AS} = \eta_a A_s f_y + \left(1 + \eta_c \frac{t}{D} \frac{f_y}{f_c}\right) A_c f_c$ $\eta_a = 0.25(3 + 2\bar{\lambda}) \leq 1$ $\eta_c = 4.9 - 18.5\bar{\lambda} + 17\bar{\lambda}^2 \geq 0$	$N_{AS} = A_s f_y + A_c f_c$

Table 4. Experimental and predicted cross-sectional strength

Series	Name	N _{exp} (kN)	EC4		AISC		DBJ		AS	
			N _{EC4} (kN)	N _{exp} / N _{EC4}	N _{AISC} (kN)	N _{exp} / N _{AISC}	N _{DBJ} (kN)	N _{exp} / N _{DBJ}	N _{AS} (kN)	N _{exp} / N _{AS}
1	C101.6x2_30	582.7	821.51	0.71	643.15	0.91	788.79	0.74	801.54	0.73
	C101.6x3_30	703.3	810.57	0.87	622.41	1.13	760.54	0.92	789.39	0.89
	C101.6x5_30	942.2	791.26	1.19	608.05	1.55	743.88	1.27	771.00	1.22
	C101.6x2_90	935.7	1172.72	0.80	997.86	0.94	1224.28	0.76	1153.56	0.81
	C101.6x3_90	1075.5	1204.95	0.89	1022.55	1.05	1250.91	0.86	1184.39	0.91
	C101.6x5_90	1311.0	1186.32	1.11	1008.26	1.30	1235.51	1.06	1166.57	1.12
2	C160x3_30	1185.7	1410.53	0.84	1074.53	1.10	1300.40	0.91	1385.05	0.86
	C160x6_30	2154.5	2718.31	0.79	1968.23	1.09	2496.32	0.86	2670.15	0.81
	C160x3_90	2021.7	2426.29	0.83	2072.60	0.98	2570.43	0.79	2400.83	0.84
	C160x6_90	2933.2	3576.52	0.82	2833.67	1.04	3660.05	0.80	3528.62	0.83
3	S125x125x3_30	824.5	1094.33	0.75	991.92	0.83	1266.98	0.65	1094.33	0.75
	S125x125x4_30	1159.2	1302.12	0.89	1202.26	0.96	1503.98	0.77	1302.12	0.89
	S125x125x3_90	1441.2	1769.24	0.81	1562.24	0.92	2104.68	0.68	1769.24	0.81
	S125x125x4_90	1882.5	1954.54	0.96	1753.63	1.07	2335.71	0.81	1954.54	0.96
4	R150x100x4_30	912.0	1052.26	0.87	969.05	0.94	1216.77	0.75	1052.26	0.87
	R150x100x5_30	1168.0	1210.94	0.96	1130.21	1.03	1412.18	0.83	1210.94	0.96
	R150x100x4_90	1188.5	1707.68	0.70	1521.79	0.78	2041.44	0.58	1707.68	0.70
	R150x100x5_90	1641.8	1824.94	0.90	1648.07	1.00	2208.37	0.74	1824.94	0.90
			Mean	0.87	Mean	1.03	Mean	0.82	Mean	0.88
			SD	0.13	SD	0.17	SD	0.16	SD	0.13

LIST OF FIGURE CAPTIONS

- Fig. 1. Concrete filled steel tubular sections studied: a) Circular; b) Square; c) Rectangular.
- Fig. 2. a) Hollow steel tubes; b) Concrete cylinder samples.
- Fig. 3. Specimens ready to be tested.
- Fig. 4. a) Scheme of test setup; b) Detail of the test setup for one of the columns (Detail A).
- Fig. 5. Typical failure mode: a) C101.6x5_90; b) S125x125x4_30.
- Fig. 6. Compression load versus shortening for: a) Series 1; b) Series 2; c) Series 3; d) Series 4.
- Fig. 7. Maximum load (N_{exp}).
- Fig. 8. Strength Index (SI).
- Fig. 9. Concrete contribution ratio (CCR).
- Fig. 10. a) Determination of ductility index from load-shortening curves; b) Ductility Index (DI).
- Fig. 11. Comparison between the predicted and measured cross-sectional strength.
- Fig. 12. Circular columns. Influence of section slenderness on code predictions.
- Fig. 13. Rectangular columns. Influence of section slenderness on code predictions.

LIST OF TABLE CAPTIONS

Table 1. Details of the column specimens and test results

Table 2. Concrete mix proportions

Table 3. Code prediction methods and limitations

Table 4. Experimental and predicted cross-sectional strength